Aalto University

OPEN ACCESS

This is an electronic reprint of the original article.
This reprint may differ from the original in pagination and typographic detail.

Pournazarian, Bahram; Sangrody, Reza; Saeedian, Meysam; Gomis-Bellmunt, Oriol; Pouresmaeil, Edris

Enhancing Microgrid Small-Signal Stability and Reactive Power Sharing Using ANFIS-Tuned Virtual Inductances

Published in:
IEEE Access

DOI:
10.1109/ACCESS.2021.3100248

Published: 26/07/2021

Document Version
Publisher's PDF, also known as Version of record

Published under the following license:
CC BY

Please cite the original version:
Pournazarian, B., Sangrody, R., Saeedian, M., Gomis-Bellmunt, O., & Pouresmaeil, E. (2021). Enhancing Microgrid Small-Signal Stability and Reactive Power Sharing Using ANFIS-Tuned Virtual Inductances. *IEEE Access*, *9*, 104915-104926. Article 9497053. https://doi.org/10.1109/ACCESS.2021.3100248

This material is protected by copyright and other intellectual property rights, and duplication or sale of all or part of any of the repository collections is not permitted, except that material may be duplicated by you for your research use or educational purposes in electronic or print form. You must obtain permission for any other use. Electronic or print copies may not be offered, whether for sale or otherwise to anyone who is not an authorised user.

IEEE Access
Multidisciplinary ⋮ Rapid Review ⋮ Open Access Journal

Received July 5, 2021, accepted July 22, 2021, date of publication July 26, 2021, date of current version August 2, 2021.

Digital Object Identifier 10.1109/ACCESS.2021.3100248

Enhancing Microgrid Small-Signal Stability and Reactive Power Sharing Using ANFIS-Tuned Virtual Inductances

BAHRAM POURNAZARIAN[1], (Student Member, IEEE), REZA SANGRODY[2], MEYSAM SAEEDIAN[1], ORIOL GOMIS-BELLMUNT[3], (Fellow, IEEE), AND EDRIS POURESMAEIL[1], (Senior Member, IEEE)

[1]Department of Electrical Engineering and Automation, Aalto University, 02150 Espoo, Finland
[2]Department of Electrical and Computer Engineering, Islamic Azad University, Firoozkooh Branch, Firoozkooh 39818-38381, Iran
[3]Centre d'Innovació Tecnològica en Convertidors Estàtics i Accionaments (CITCEA-UPC), Departament d'Enginyeria Elèctrica, Universitat Politècnica de Catalunya, 08028 Barcelona, Spain

Corresponding author: Edris Pouresmaeil (edris.pouresmaeil@aalto.fi)

ABSTRACT Microgrid as the main building block for future smart grids is prone to instability originated from converter-based distributed generations (DG). Herein, we first analyze the small-signal stability of an inverter-interfaced microgrid. Afterwards, a novel adaptive network fuzzy inference system (ANFIS)-based optimization method is introduced which aims at online tuning of virtual inductances (VI) in the islanded microgrids. The data for ANFIS training is drawn by particle swarm optimization (PSO) algorithm and the proposed objective function. A total of 140 load scenarios are considered to provide optimal VI in each load condition and generate optimal data for ANFIS training. This process minimizes reactive power mismatches and improves microgrid stability in different load levels. The simultaneous application of PSO algorithm and ANFIS training facilitates the objectives pursued by current study. Finally, the trained ANFIS networks are installed in the converter control. The adaptive performance of ANFIS controllers makes the converters responses independent from load change location and value. The effectiveness of the proposed control methodology is verified using simulations studies.

INDEX TERMS Adaptive network fuzzy inference system (ANFIS), microgrid, particle swarm optimization (PSO), small-signal stability, virtual inductance (VI).

NOMENCLATURE

ABBREVIATIONS

ANFIS	Adaptive network fuzzy inference system
DG	Distributed generation
ESS	Energy storage system
FIS	Fuzzy inference systems
LPF	Low-pass filter
MFs	Membership functions
Nadir	Point of minimum frequency
PBDG	Power electronic-based distributed generation
PLL	Phase-locked loop
PSO	Particle swarm optimization
PI	Proportional integral
VI	Virtual inductances

VARIABLES

v_{odq}	Converter's output voltage components in dq frame
v_{bDQ}	Bus voltage components in common dq frame
i_{odq}	Converter's output current components in dq frame
i_{ldq}	Converter's terminal current components in dq frame
p, q	Instantaneous active and reactive powers of converter
P, Q	Active and reactive powers of Converter
ω_{PLL}	Angular frequency measured by PLL
φ_{PLL}	Ancillary state variable used in PLL modeling
δ_i	Angle between d-axis of i^{th} and 1^{st}

PARAMETERS

ζ	Damping ratio of an eigenvalue
ω_c	Cut-off frequency of low-pass filter

The associate editor coordinating the review of this manuscript and approving it for publication was Guangdeng Zong.

This work is licensed under a Creative Commons Attribution 4.0 License. For more information, see https://creativecommons.org/licenses/by/4.0/

ω_n	Nominal angular frequency of MG
$\omega_{c,PLL}$	Cut-off frequency of low-pass filter in PLL
n	Reactive power droop coefficient
L_v	Virtual inductance
MaxIt	Number of iterations in PSO
nPop	Population size (swarm size) in PSO
ω	Inertia weight in PSO
c_1	Personal learning coefficient in PSO
c_2	Global learning coefficient in PSO
Lv_{min}	Lower bound of virtual inductance
Lv_{max}	Upper bound of virtual inductance
f_{sw}	PWM switching frequency

I. INTRODUCTION

The global energy revolution aims at utilizing green energy resources and highlights the potential challenges of future converter-interfaced microgrids. A microgrid is basically a non-linear dynamic system including power electronic-based distributed generations (PBDG), energy storage systems (ESS) and static/dynamic loads. A microgrid can be either a part of a host power system or can be an autonomous energy supplier for a remote load. The stability of a microgrid is defined as the ability of a microgrid to attain new steady-state values for the state variables after being subjected to a small-signal disturbance [1]. The first step to study the microgrid stability is to model the microgrid as a non-linear control system based on the modeling of different elements and then to linearize the dynamic equations around the operating point [2].

Multiple converters in microgrid can be controlled on a common synchronous reference frame (dq) based on droop control [3]. The boundary of stability region of a distributed generation (DG) is estimated by Kernel Ridge Regression method [4]. In [5], a trade-off exists between load-sharing and microgrid stability and a power system stabilizer (PSS) is proposed to damp the low-frequency oscillations at higher droop values [5]. The performance of a microgrid under harmonic conditions originated from nonlinear loads is upgraded by a novel virtual impedance control methodology [6]. A detailed modeling of the microgrid is a necessity for a precise small-signal stability analysis and the dynamics of different elements such as phased-lock loop (PLL) should be considered [7].

From stability point of view, the dynamic performance of model-based voltage and current controller is much more better than the conventional proportional-integral (PI) controllers but this method does not deal with the reactive power sharing problem in microgrid [8]. Microgrid stability analysis under distributed control is performed by a theoretical framework in [9]; however, the communication latency and microgrid topology affect the performance of this method.

The small-signal modeling of microgrid clusters, the participation factors analysis for lower-damped modes, and the sensitivity analysis for control parameters are accomplished in [10]; nonetheless, the communication requirements between converters has been a drawback for this study. The dynamic droop control method proposed in [11] has improved the transient response and the stability of the microgrid. On the other hand, this method has tuned the controllers off-line and its performance might not be optimal in all operating points. The inverters stability prediction is proposed in [12] based on a new terminal characteristic modeling for parallel droop-controlled inverters. However, this method does not deal with reactive power mismatches issue. The permissible intervals for microgrid parameters in presence of current state feedback can be determined using small-signal stability analysis in [13].

The dynamic responses of single-loop and multi-loop droop control methods are analyzed and compared in [14] by microgrid small-signal stability analysis, but it does not deal with reactive power sharing problem. The bifurcation theory is used in [15] to analyze the parameters stability region in an islanded microgrid supplying static and dynamic loads. However, the model of microgrid does not include PLL and the fair reactive power sharing could not be ensured. The internal model control (IMC) optimization has enhanced the dynamic performances of DGs, but still the reactive power sharing has not been resolved in [16].

On the other hand, the reactive power sharing among several converters and the power coupling problems highlight the virtual impedance concept in a MG. The microgrid stability, transient sharing of current and power between inverters, and voltage and current harmonics can be enhanced by virtual impedances. However, the inappropriate tuning of virtual impedances can lead to micogrid instability and unfavorable voltage drops. A robust virtual impedance method is proposed in [17] to decrease the voltage distortion caused by harmonic loads. This method has facilitated the power control during the faults. Though, the proposed converter model is a simplified model and lacks the essential components such as voltage control, current control, and PLL. A systematic method to draw feasible ranges of virtual impedances is introduced in [18] to enhance power decoupling, microgrid damping, and voltage profile, simultaneously. This off-line optimization method does not ensure a fair reactive power sharing in all operating points.

The virtual impedance optimization in [19] has minimized the reactive power mismatches among converters and enhanced the microgrid small-signal stability by an off-line PSO algorithm. Following the analysis of microgrid stability domain in [20], it has been suggested that the proportional-derivative reactive power controller enhances the microgrid stability margin. The proposed converter model has lacked any mechanism to deal with reactive power sharing issue.

A power oscillation damper based on artificial intelligent is suggested in [21] for grid-forming converters to mitigate the electromechanical power oscillation. The learning capability of adaptive network-based fuzzy inference system (ANFIS) constructs a mapping between inputs and outputs in the form of fuzzy if-then rules [22]. The double artificial neural

network (ANN) based strategy is proposed in [23] to enhance the stability and reliability of virtual synchronous generators (VSGs).

Another application of ANFIS is proposed in [24] to control voltage and frequency of microgrid in different load levels, simultaneously. The islanding detection for PBDG is proposed in [25] by utilizing the pattern recognition capability of ANFIS. Moreover, ANFIS-based controllers are devised in [26] to cope with the voltage compensation in a low-voltage microgrid including several voltage source converters and unbalanced loads. Considering the previous literature review, the following research gaps are observed:

- The permissible range and optimal values for virtual impedance are affected by the microgrid load levels, this concept has not been considered in the recent researches such as [18] and [19].
- The application of ANFIS in online tuning of VI to enhance the microgrid small-signal stability has not been covered.
- The adaptive tuning of virtual impedances considering the microgrid stability and reactive power sharing in different load levels has not been well-focused.

Consequently, the following contribution are introduced for this research work:

- The online ANFIS-based optimization of VI is proposed and devised resulting in minimum reactive power mismatches in all load scenarios, enhanced microgrid small-signal stability and negligible voltage drops.
- The optimal VI values are calculated for 140 different load levels and this optimal values are applied as the training data for ANFIS controllers. The suggested ANFIS controller is independent of microgrid configuration and load change.

The next sections of this paper are presented as follows; the microgrid modeling is introduced in section II. The small-signal stability analysis of the microgrid under study is elaborated in section III. The proposed ANFIS-based optimization algorithm is introduced in section IV. The simulation results and conclusions are brought in sections V and VI, respectively.

II. MICROGRID MODELING

The control block diagram of a PBDG supplying a static load is depicted in Fig. 1. It is assumed that several PBDG units are sharing the power based on traditional droop control in an islanded MG. The control methodology is implemented on a global dq frame [2]. The global reference frame could either be synchronized with one of the local PBDGs or an external angle reference. Different blocks such as power calculator, droop controller, voltage controller, current controller, and PLL seen in Fig. 1 are explained as follows.

A. POWER CALCULATOR

Two instantaneous power components (p, q) are calculated in dq-reference frame and then pass through a low-pass

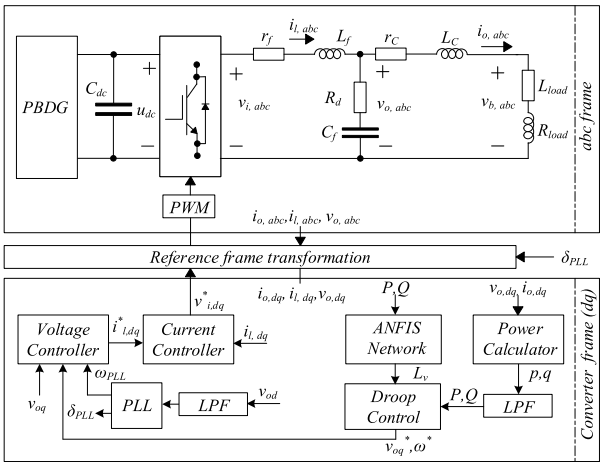

FIGURE 1. The control block diagram of an interface converter in islanded microgrid.

filter (LPF) with the cut-off frequency of ω_c and the active and reactive power are calculated afterwards [2].

$$P = (\frac{3}{2}).(\frac{\omega_c}{s+\omega_c}).\underbrace{(v_{od}.i_{od} + v_{oq}.i_{oq})}_{p} \tag{1}$$

$$Q = (\frac{3}{2}).(\frac{\omega_c}{s+\omega_c}).\underbrace{(v_{oq}.i_{od} - v_{od}.i_{oq})}_{q} \tag{2}$$

B. DROOP CONTROL

Droop equations for the frequency and voltage control are applied in dq reference frame to assign the frequency and voltage references. The reference frequency is calculated by droop equation (3), in which ω_n and m are nominal frequency of microgrid and active power droop coefficient, respectively. The dq-axis voltage components are calculated by (4). The voltage reference is obviously affected by the value of virtual reactance (L_v) which are later calculated online by ANFIS controller.

$$\omega^* = \omega_n - m.P \tag{3}$$

$$v^*_{oq} = v_{qN} - n.Q - (\omega_n.L_v.i_{oq})$$
$$v^*_{od} = 0 \tag{4}$$

where v_{qN}, n, and L_v are nominal q-axis voltage, reactive power droop coefficient, and virtual inductance, respectively.

C. VOLTAGE CONTROLLER

The voltage controller unit assigns the current references in terms of instantaneous voltage and frequency values. Two first order dynamic equations calculate the dq current references as follows [7]:

$$i^*_{ld} = k_{iv}.\varphi_d + k_{pv}.\underbrace{(\omega_{PLL} - \omega^*)}_{\dot{\varphi}_d}$$

$$i^*_{lq} = k_{iv}.\varphi_q + k_{pv}.\underbrace{(v^*_{oq} - v_{oq})}_{\dot{\varphi}_q} \tag{5}$$

where k_{pv} and k_{iv} are proportional and integral coefficients of proportional-integral (PI) controller utilized in voltage controller. Moreover, ω_{PLL}, v^*_{oq}, and ω^* are the angular frequency measured by PLL, q-axis voltage reference, and reference angular frequency, respectively.

D. CURRENT CONTROLLER

The current controller compares instantaneous current components with current references and generates reference voltage components for PWM block accordingly.

$$v^*_{id} = -\omega_n.L_f.i_{lq} + k_{ic}.\gamma_d + k_{pc}.\underbrace{(i^*_{ld} - i_{ld})}_{\dot{\gamma}_d} \quad (6)$$

$$v^*_{iq} = \omega_n.L_f.i_{ld} + k_{ic}.\gamma_q + k_{pc}.\underbrace{(i^*_{lq} - i_{lq})}_{\dot{\gamma}_q} \quad (7)$$

where k_{pc} and k_{ic} are the proportional and integral coefficient of PI controller and γ is an auxiliary variable to simplify the formulation.

E. PLL MODEL

The phase-locked loop (PLL) measures the phase shift of fundamental component of voltage. A PLL model has been introduced in [7] which utilizes two PI controllers with the coefficients of $k_{p,PLL}$ and $k_{i,PLL}$ in dq reference frame. The PLL model in current study determines the phase angle so as v_{od} is zero in steady-state. The PLL model in some other studies such as [2] and [8], forces v_{oq} to become zero. There is not any difference, neither in the concept nor in the performance. The intention to apply PLL model in [7] has been its simplicity and these similar PLL models facilitate the comparison of research results with this reference, e.g. v_{od} in this study is compared with v_{od} in [7], similar idea holds for v_{oq}.

$$\dot{v}_{od,f} = \omega_{c,PLL}.v_{od} - \omega_{c,PLL}.v_{od,f} \quad (8)$$

$$\dot{\varphi}_{PLL} = -v_{od,f} \quad (9)$$

$$\dot{\delta}_{PLL} = \omega_{PLL} \quad (10)$$

$$\omega_{PLL} = \omega_n - k_{p,PLL}.v_{od,f} + k_{i,PLL}.\varphi_{PLL} \quad (11)$$

III. SMALL-SIGNAL STABILITY ANALYSIS

A. STATE-SPACE REPRESENTATION OF THE MICROGRID

The following state variables are considered in this study for the 3-bus test microgrid (Fig.2) and the corresponding state-space equations are drawn afterwards. It should be noted that the reference frame of converter 1 is chosen as global dq frame.

$$\begin{aligned} x = [&\delta_1, P_1, Q_1, \phi_{d1}, \phi_{q1}, \gamma_{d1}, \gamma_{q1}, i_{ld1}, i_{lq1}, v_{od1}, v_{oq1},\\ &i_{od1}, i_{oq1}, \varphi_{PLL1}, v_{od,f1}, \delta_2, P_2, Q_2, \phi_{d2}, \phi_{q2}, \gamma_{d2}, \gamma_{q2},\\ &i_{ld2}, i_{lq2}, v_{od2}, v_{oq2}, i_{od2}, i_{oq2}, \varphi_{PLL2}, v_{od,f2}, \delta_3, P_3,\\ &Q_3, \phi_{d3}, \phi_{q3}, \gamma_{d3}, \gamma_{q3}, i_{ld3}, i_{lq3}, v_{od3}, v_{oq3}, i_{od3}, i_{oq3},\\ &\varphi_{PLL3}, v_{od,f3}, i_{loadD1}, i_{loadQ1}, i_{loadD2}, i_{loadQ2}, i_{loadD3},\\ &i_{loadQ3}, i_{lineD1}, i_{lineQ1}, i_{lineD2}, i_{lineQ2}] \end{aligned} \quad (12)$$

$$\dot{\delta}_1 = \omega_{PLL1} - \omega_{PLL1} = 0 \quad (13)$$

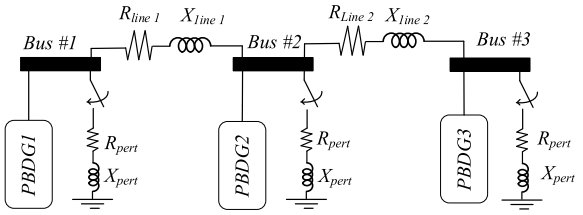

FIGURE 2. The 3-bus test MG.

where ω_{PLL1} is the angular frequency (rad/s) measured by the PLL at bus 1.

The state equations for active and reactive power injected by converter 1 are written as (14) and (15), respectively.

$$\dot{P}_1 = 1.5\omega_c(v_{od1}.i_{od1} + v_{oq1}.i_{oq1}) - \omega_c.P_1 \quad (14)$$

$$\dot{Q}_1 = -1.5\omega_c(v_{od1}.i_{oq1} - v_{oq1}.i_{od1}) - \omega_c.Q_1 \quad (15)$$

The state equation (16) and (17) aim at auxiliary variables (ϕ_{d1} and ϕ_{q1}) which are used to simplify the formulations and ω^*_1 is the frequency reference of converter 1, which is calculated by droop control (3).

$$\dot{\phi}_{d1} = \omega_{PLL1} - \omega^*_1 \quad (16)$$

$$\dot{\phi}_{q1} = v^*_{oq1} - v_{oq1} = v_{qN} - n.Q_1 - X_{v1}.i_{od1} \quad (17)$$

where v^*_{oq1}, v_{qN}, n, and X_{v1} are q-axis voltage reference, q-axis nominal voltage, reactive power droop coefficient, and virtual reactance, respectively.

The auxiliary variables γ_{d1} and γ_{q1} are explained by state-equations (18) and (19), respectively.

$$\dot{\gamma}_{d1} = i^*_{ld1} - i_{ld1} = k_{iv}.\phi_{d1} + k_{pv}.(\omega_{PLL1} - \omega^*_1) - i_{ld1} \quad (18)$$

$$\dot{\gamma}_{q1} = i^*_{lq1} - i_{lq1} = k_{iv}.\phi_{q1} + k_{pv}.(v^*_{oq1} - v_{oq1}) - i_{lq1} \quad (19)$$

The state equations (20) and (21) aim at calculating terminal current components for the converter 1 (i_{ld1}, i_{lq1}) while r_f, v^*_{id1} and v^*_{iq1} are output resistance of converter, d and q-axis voltage references dictated to the PWM unit. It is assumed that the converter is lossless and the PWM voltage command appears exactly at terminal of the converter.

$$\dot{i}_{ld1} = \frac{1}{L_f}(-r_f.i_{ld1} + v^*_{id1} - v_{od1}) + \omega_{PLL1}.i_{lq1} \quad (20)$$

$$\dot{i}_{lq1} = \frac{1}{L_f}(-r_f.i_{lq1} + v^*_{iq1} - v_{oq1}) - \omega_{PLL1}.i_{ld1} \quad (21)$$

The dq voltage components of the converter 1 (v_{od1}, v_{oq1}) are provided in (22) and (23) while C_f and R_d are filtering capacitance and damping resistance, respectively [7].

$$\dot{v}_{od1} = \frac{1}{C_f}(i_{ld1} - i_{od1}) + \omega_{PLL1}.v_{oq1} + R_d.(\dot{i}_{ld1} - \dot{i}_{od1}) \quad (22)$$

$$\dot{v}_{oq1} = \frac{1}{C_f}(i_{lq1} - i_{oq1}) - \omega_{PLL1}.v_{od1} + R_d.(\dot{i}_{lq1} - \dot{i}_{oq1}) \quad (23)$$

The output dq-current components of the converter 1 (i_{od1}, i_{oq1}) are explained by (24) and (25), respectively.

$$\dot{i}_{od1} = \frac{1}{L_c}(-r_c.i_{od1} + v_{od1} - v_{bd1}) + \omega_{PLL1}.i_{oq1} \quad (24)$$

$$\dot{i}_{oq1} = \frac{1}{L_c}(-r_c.i_{oq1} + v_{oq1} - v_{bq1}) - \omega_{PLL1}.i_{od1} \quad (25)$$

where r_c and L_c are resistance and inductance of output branch of LCL filter as seen in Fig.1 and v_{bd1} and v_{bq1} are the dq components of voltage at bus 1, which are calculated by (26) using the virtual resistor method [2]. It should be noted that all variables with DQ indices (e.g. i_{loadD1}, i_{lineD1}) are presented in global reference frame. The reference frame of converter 1 is chosen as global reference frame and the transformation between local and global frames are explained in [7].

$$\begin{aligned} v_{bd1} &= r_n(i_{od1} - i_{loadD1} - i_{lineD1}) \\ v_{bq1} &= r_n(i_{oq1} - i_{loadQ1} - i_{lineQ1}) \end{aligned} \quad (26)$$

The state equation for φ_{PLL1} is (27) in which the PLL model tends to force the d-axis voltage to zero.

$$\dot{\varphi}_{PLL1} = -v_{od,f1} \quad (27)$$

The last state equation describing converter 1 is (28) which aims at d-axis voltage of PLL after LPF ($v_{od,f1}$) and $\omega_{c,PLL}$ is the cut-off frequency of LPF.

$$\dot{v}_{od,f1} = \omega_{c,PLL}.(v_{od1} - v_{od,f1}) \quad (28)$$

The state-equations for static loads can be drawn by a similar method as described in [3]. Here, the state equations for load 1 at bus 1 are written as (29) and (30) and the same equations for load 2 and load 3 are drawn straightforwardly by similar calculations.

$$\dot{i}_{loadD1} = \frac{1}{L_{load1}}(-R_{load1}.i_{loadD1} + v_{bd1}) + \omega_{PLL1}.i_{loadQ1} \quad (29)$$

$$\dot{i}_{loadQ1} = \frac{1}{L_{load1}}(-R_{load1}.i_{loadQ1} + v_{bq1}) - \omega_{PLL1}.i_{loadD1} \quad (30)$$

where R_{load1} and L_{load1} have been resistance and inductance of static load 1. The state equations for line 1 which is between bus 1 and bus 2 are written as (31) and (32). For line 2, the state equations can be drawn similarly.

$$\dot{i}_{lineD1} = \frac{1}{L_{line1}}(-R_{line1}.i_{lineD1} + v_{bd1} - v_{bD2}) + \omega_{PLL1}.i_{lineQ1} \quad (31)$$

$$\dot{i}_{lineQ1} = \frac{1}{L_{line1}}(-R_{line1}.i_{lineQ1} + v_{bq1} - v_{bQ2}) - \omega_{PLL1}.i_{lineD1} \quad (32)$$

where R_{line1} and L_{line1} are the resistance and the inductance of line 1, and v_{bD2} and v_{bQ2} are the bus 2 voltage in global reference frame. The calculation of bus voltages in global reference frame can be found in similar research such as [7] and [2]. Once the state-space equations for all converters, lines, and loads are written, the corresponding set of non-linear differential equations are linearized around an stable operating point and then a state matrix including numeric coefficients (A) is drawn.

$$\Delta\dot{x} = A.\Delta x \quad (33)$$

Then the following MATLAB command is used to draw the eigenvalues of microgrid.

$$\lambda = eig(A) \quad (34)$$

B. EIGENVALUES ANALYSIS

Since the microgrids are of high order and have several modes with different damping ratios, their transfer functions are too complicated. However, the major eigenvalues analysis is a well-known method to examine the small-signal stability of microgrids. The dominant eigenvalues of 3-bus test microgrid either drawn by the proposed ANFIS-based controller or applying the control method in [7] for an stable operating point (R_{load1}=R_{load2}=R_{load3}=50Ω) are demonstrated in Fig.3. The specifications of the converters are listed in Table 1. The minimum real parts of microgrid eigenvalues are -7.24 and -1.41 while applying the ANFIS-based proposed controller and the controller in [7], respectively. Therefore, the real part of dominant eigenvalues is enhanced by the proposed control method. On the other hand, the minimum damping ratio corresponding to the worst eigenvalue in Fig.3 are increased from 14.84 % to 33.94 % using the proposed control method. Consequently, the small-signal stability of microgrid is enhanced prominently by the proposed control method.

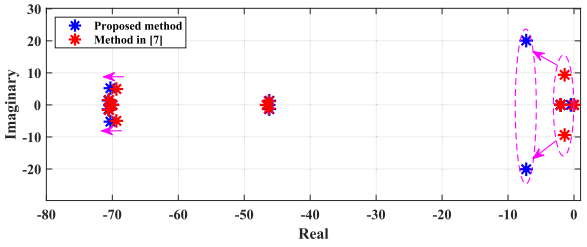

FIGURE 3. The 3-bus microgrid dominant eigenvalues while applying the proposed ANFIS-based method and the control method in [7].

C. ANALYSIS OF VIRTUAL INDUCTANCES EFFECTS ON MICROGRID SMALL-SIGNAL STABILITY

The virtual inductances in (4) facilitate the fair reactive power sharing among multiple converters by regulating the bus voltages. On the other hand, inappropriate choice of virtual inductances can jeopardize the microgrid small signal stability by propelling microgrid eigenvalues towards right half-plain. As the eigenvalues participation analysis in [7] reveals, the weakest eigenvalues with minimum damping ratios are mostly affected by bus voltages. Therefore it is

TABLE 1. Converters parameters.

Parameter	Value	Parameter	Value
L_f, C_f	$1.35\ mH, 50\ \mu F$	r_f, r_n	$0.1\ \Omega, 1000\ \Omega$
U_{dc}	$650\ V$	f_{sw}	$6\ kHz$
r_c, ω_c	$0.03\ \Omega, 70\ rad/s$	L_c, ω_n	$0.35\ mH, 314\ rad/s$
$\omega_{c,PLL}$	$7853.98\ rad/s$	m, n	0.000094, 0.0013
V_{oqN}, ω_n	$380\ V, 314\ rad/s$	R_d	$5\ \Omega$
R_{pert}	$25\ \Omega$	L_{pert}	$0.1\ mH$
R_{line1}	$0.23\ \Omega$	X_{line1}	$0.1\ \Omega$
R_{line2}	$0.35\ \Omega$	X_{line2}	$0.58\ \Omega$
$k_{p,PLL}$	0.25	$k_{i,PLL}$	2
k_{pv}, k_{iv}	1, 45	k_{pc}, k_{ic}	10.5, 1600

expected that virtual inductances which are directly changing the bus voltages seriously affect the small-signal stability of microgrid. However, the virtual inductances also affect the reactive power sharing among converters and the role of reactive powers on microgrid small-signal stability have been verified in [2], [8]. Consequently, both the reactive power sharing and microgrid small-signal stability are considered while tuning the virtual inductances. In order to clarify the role of virtual inductances on small-signal stability of the 3-bus test microgrid (Fig.2). It is assumed that an equal resistive load (50 Ω) is installed at all three buses.

The virtual inductances are changed from 0 to 0.05 H and three dominant clusters of eigenvalues are depicted in Fig.4. As it is seen in Fig.4a, by increasing L_{v1} a complex eigenvalue is moved from $-1.41 \pm$ j9.39 to $-0.15 \pm$ j10.18 and the other eigenvalue is displaced from -0.05 to -0.7 (cluster 1). Consequently, increasing L_{v1} worsens the small-signal stability of 3-bus test microgrid. Fig.4b demonstrates the dominant eigenvalues of the 3-bus test microgrid while changing L_{v2} from 0 to 0.05 H. A pair of complex eigenvalues are moved from -1.41 ± 9.39 to -25.52 ± 29.46 (cluster 1). Therefore, by increasing L_{v2}, the small-signal stability of microgrid is enhanced. By increasing L_{v3} in Fig.4c, the dominant eigenvalue is displaced from -0.05 to -0.6 (cluster 1). Accordingly, the increase in L_{v3} enhances the small-signal stability of 3-bus test microgrid.

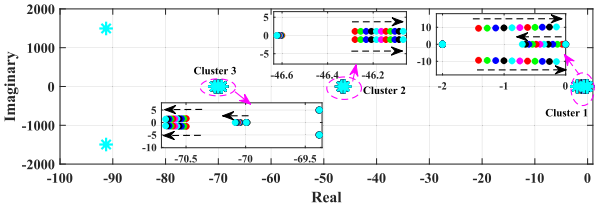

(a) L_{v1} changes from 0 to 0.05 H.

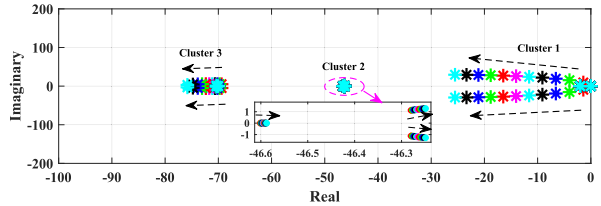

(b) L_{v2} changes from 0 to 0.05 H.

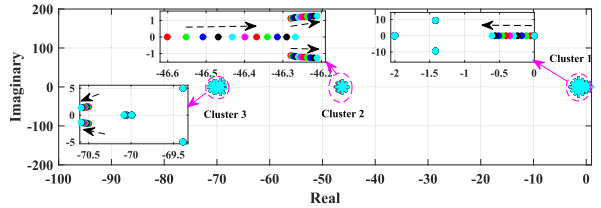

(c) L_{v3} changes from 0 to 0.05 H.

FIGURE 4. The dominant eigenvalues of 3-bus test microgrid while changing virtual inductances.

IV. THE PROPOSED ANFIS-BASED OPTIMIZATION ALGORITHM

The application of ANFIS to train a generalized controller can be found in several researches such as [24]- [26]. The idea is that the ANFIS network is trained to perform optimally in all operating conditions. The training data is produced by PSO optimization in different load changing scenarios [19]. When the training data is collected, ANFIS networks are trained for all converters in microgrid. The subsequent subsections explain the operational steps.

A. THE PROPOSED OBJECTIVE FUNCTION

The PSO algorithm is applied to minimize an objective function (O.F.). First of all, this objective function should be introduced. The damping ratio of an eigenvalue is defined by (35) in terms of its real and imaginary parts [3].

$$\zeta(Z = Re + j.Im) = \frac{|\ Re\ |}{\sqrt{(Re^2 + Im^2)}} \tag{35}$$

The number of microgrid eigenvalues is assumed to be m and the number of operating points are p. The worst damping ratio of microgrid is the minimum damping ratio among all operating points defined by (36).

$$\zeta_{worst} = \text{minimum}\{\zeta^1_{min}, \zeta^2_{min}, \ldots, \zeta^p_{min}\} \tag{36}$$

Another concern of this research is to deal with reactive power mismatches which are calculated by (37).

$$\Delta Q = \sum_{j=1}^{n-1} |\ \frac{n_j.Q_j - n_{j+1}.Q_{j+1}}{Q_N}\ | \tag{37}$$

where n_j, n, Q_j, and Q_N are reactive power droop coefficient of j^{th} converter, the number of converters in microgrid, the reactive power of j^{th} converter, and the base reactive power, respectively. The proposed objective function (38) aims at minimizing the reactive power mismatches and enhancing the small-signal stability of microgrid. Since the least-damped eigenvalues are mostly affected by voltage components (v_{od}, v_{oq}) and at the same time the VI are used in voltage loop to fairly share the reactive power, the idea is to consider microgrid stability and reactive power sharing in the proposed multi-objective function (38). The arbitrary weighting coefficient (α) is considered to determine the share

of any agent in (38).

$$\text{O.F.} = \alpha.\Delta Q + (1-\alpha)(1-\zeta_{worst}) \quad 0 \leqslant \alpha \leqslant 1 \quad (38)$$

B. THE PROPOSED FLOWCHART FOR ANFIS NETWORKS TRAINING

In order to train ANFIS networks which are seen in control block diagram in Fig.1, the flowchart of Fig.5 is proposed. This flowchart is explained in nine successive steps. The PSO algorithm has been well-explained in several researches such as [26], [27].

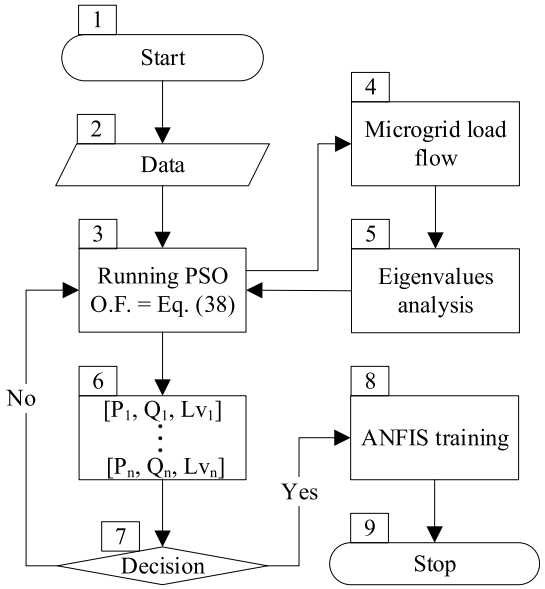

FIGURE 5. The proposed method for training ANFIS networks.

- *Step 1:* The PSO algorithm is initiated by entering the number of iterations (*Iter*), the inertia weight (w), number of population (*nPop*), number of variables (*nVar*), positive constants (c_1, c_2), weighting coefficient (α), and permissible intervals for variables [27]. The PSO algorithm specifications are listed in Table 2.

TABLE 2. PSO algorithm parameters.

Parameter	Value	Parameter	Value
$Iter, w$	100, 0.7298	$nPop, nVar$	10, 3
c_1, c_2	0.1, 1.4962	α	0.5
$L_{v1,min}$	0 H	$L_{v1,max}$	0.05H
$L_{v2,min}$	0 H	$L_{v2,max}$	0.05 H
$L_{v3,min}$	0 H	$L_{v3,max}$	0.05 H

- *Step 2:* The microgrid data including load scenarios and controller parameters are entered based on the specifications listed in Table. 1.
- *Step 3:* The PSO algorithm is run, while the objective function (38) is applied. The optimization variables are playing the roles of particles in PSO, as it is seen in (39).

$$y = [L_{v1}, \ldots, L_{vn}] \quad (39)$$

The PSO particles in any iteration are updated by (40) where the velocity of this transition is calculated by (41) [27].

$$y_i^{(k+1)} = y_i^{(k)} + V_i^{(k+1)} \quad (40)$$

where $y_i^{(k+1)}$, $y_i^{(k)}$, and $V_i^{(k+1)}$ are the particle location in iteration $k+1$, the particle location in iteration k, and the velocity of i^{th} particle in iteration $k+1$, respectively.

$$V_i^{(k+1)} = \omega.V_i^{(k)} + r_1.c_1(P_i^{(k)} - y_i^{(k)}) + r_2.c_2(P_{best}^{k} - y_i^{(k)}) \quad (41)$$

where $P_i^{(k)}$ is the value of objective function for i^{th} particle in k^{th} iteration which is calculated by (38) and P_{best}^{k} is the minimum value of objective function among all population in k^{th} iteration. The particles locations are limited by minimum ($y_{i,min}$) and maximum ($y_{i,max}$) permissible values. This condition can be written as follows (42).

$$y_i^{(k)} = min\{max(y_i^{(k)}, y_{i,min}), y_{i,max})\} \quad (42)$$

- *Step 4:* The microgrid load-flow is run and depending on the time-step, several operating points are drawn for the microgrid.
- *Step 5:* The eigenvalues analysis for all operating points is accomplished and the eigenvalue with minimum damping ratio is determined. If any of the eigenvalues has a positive real part, that PSO solution is not feasible and therefore is removed.
- *Step 6:* The optimal data set for any converter in the microgrid includes its active power, reactive power, and optimal virtual inductance. A three bus test microgrid which is shown in Fig.2 is considered. All optimal data sets are saved for all load scenarios of Fig.6 as a matrix $[D]_{140\times 9}$.

$$D = \begin{bmatrix} P_1^1 & Q_1^1 & L_{v1}^1 & \ldots & P_3^1 & Q_3^1 & L_{v3}^1 \\ \vdots & \vdots & \vdots & \ddots & \vdots & \vdots & \vdots \\ P_1^{140} & Q_1^{140} & L_{v1}^{140} & \ldots & P_3^{140} & Q_3^{140} & L_{v3}^{140} \end{bmatrix} \quad (43)$$

- *Step 7:* The load scenarios which are seen in Fig.6 are run and 140 set of optimal data-sets are prepared. For instance, in scenario 1 the load at bus 1 is 1 p.u. (R_{pert}= 50 Ω and L_{pert}= 50 mH) and the loads at bus 2 and 3 are 0 kW. Subsequently, in scenario 2 the load at bus 1 is R_{pert}= $\frac{50}{0.95}$ Ω and L_{pert}= $\frac{0.050}{0.95}$ H and the loads at buses 2 and 3 are 0 kW and 0 kVAR. The values of R_{pert} and L_{pert} in other scenarios can be drawn similarly by Fig.6 which change by 0.05 in any step. If all 140 data sets are prepared, the data matrix (D) is ready and the algorithm can succeed to step 8, otherwise the next load scenario is run by starting from step 3.
- *Step 8:* Training capability of artificial neural networks and the fuzzy logic are gathered in ANFIS. The input/output mapping with membership functions (*MFs*) is performed based on fuzzy rules to generate

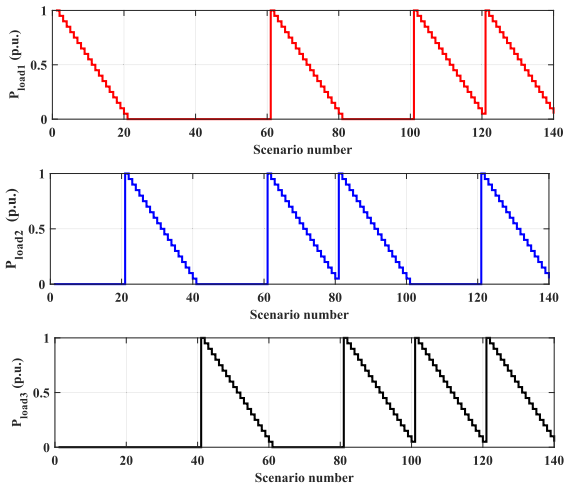

FIGURE 6. The load change scenarios used for ANFIS networks training.

I/O pairs [24]. The ANFIS training requires a set of training data. The command *anfisedit* in MATLAB environment calls the MATLAB neuro-fuzzy designer as a straightforward tool to train ANFIS controllers. The inputs and outputs values should be written in the same matrix. For instance, in order to train an ANFIS network for L_{v1}, columns 1-3 matrix $[D]_{140\times9}$ are used as the training data. Moreover, columns 4-6 and 7-9 of matrix $[D]_{140\times9}$ are used to train L_{v2} and L_{v3}, respectively. Full specifications of ANFIS networks are listed in Table.3.

- *Step 9:* The trained ANFIS networks are installed in converter control block-diagram of Fig.1.

V. SIMULATION RESULTS

A 3-bus test microgrid is implemented as seen in Fig.2. Details of the MG are found in Table. 1. Firstly, the sensitivity of reactive power mismatches and the damping of worst eigenvalue with respect to α are scrutinized. Then the ANFIS networks are trained by the proposed algorithm. The ANFIS toolbox in MATLAB is used and the ANFIS networks specifications are listed in Table.3. Finally the load change scenario is implemented and the dynamic characteristics of microgrid are verified.

TABLE 3. ANFIS networks parameters.

Parameter	Value or Type	Parameter	Value or Type
Number of MFs	3, 3	MF type	trimf, constant
Epochs	50	Error tel.	0.0001
FIS training	Grid partition	Optim. Method	hybrid

A. SENSITIVITY ANALYSIS

The loads at buses 1 and 3 are $R_{pert} = 25\ \Omega$ and there is no load at bus 2. The weighting coefficient (α) in the objective function (38) affects the share of any participant. The value of α is changed from 0 to 1 and the optimal values of optimal virtual inductances are determined by steps 1-7 of the proposed algorithm (Fig.5). The bigger values of α lead to lower reactive power mismatches and lower values of α enhance the stability of microgrid by enhancing the damping of worst eigenvalue. As Fig.7a demonstrates, the maximum reactive power mismatch is seen at $\alpha = 0$. By increasing α the reactive power mismatches decreases. It should be noted that for the $\alpha > 0.5$ the rate of drop in reactive power mismatch is negligible.

The damping ratio percentage of the worst eigenvalue is shown in Fig.7b for different values of α. It is seen that for $\alpha = 0$ the damping ratio of worse eigenvalue is 37.62% which is the maximum possible value. By increasing α the damping ratio of worst eigenvalue decreases gradually. The rate of reducing the damping ratio for $\alpha > 0.5$ is negligible.

Consequently, choosing $\alpha = 0.5$ is a good compromise for the multi objective equation (38) to have a relatively low reactive power mismatch and a high minimum damping ratio.

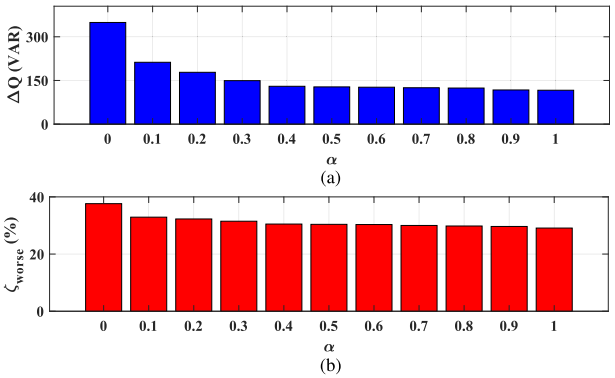

FIGURE 7. The sensitivity analysis for reactive power mismatches and the damping of worst eigenvalue of microgrid with respect to weighting factor (α).

B. TRAINING ANFIS NETWORKS

There are three converters in the 3-bus test microgrid and three ANFIS networks are required in the control block-diagram. A two-input one-output ANFIS network is trained for any converter by MATLAB. The MATLAB command *anfisedit* loads the ANFIS training toolbox. The full specifications of ANFIS networks are listed in Table.3. The active power and the reactive powers are inputs and virtual inductance is the output which are placed in first, second, and third column of a matrix, respectively. The data sets include 140 load scenarios. The ANFIS network for L_{v1}, L_{v2}, L_{v3} are depicted in Fig.8. The virtual inductance L_{v1} in Fig.8a shows two opposite trends around $P_1 = 4583.1\ W$, before and after this point the virtual inductance value shows a drop and a growth by a rise in active power, respectively.

The ANFIS network for L_{v2} in Fig.8b demonstrates roughly a direct relationship between the value of P_2 and the value of L_{v2}. However, the plain slope in $Q_2 - L_{v2}$ axis has a breaking point ($Q_2 = 975.36\ VAR$). Before and after this point the slopes have positive and negative values.

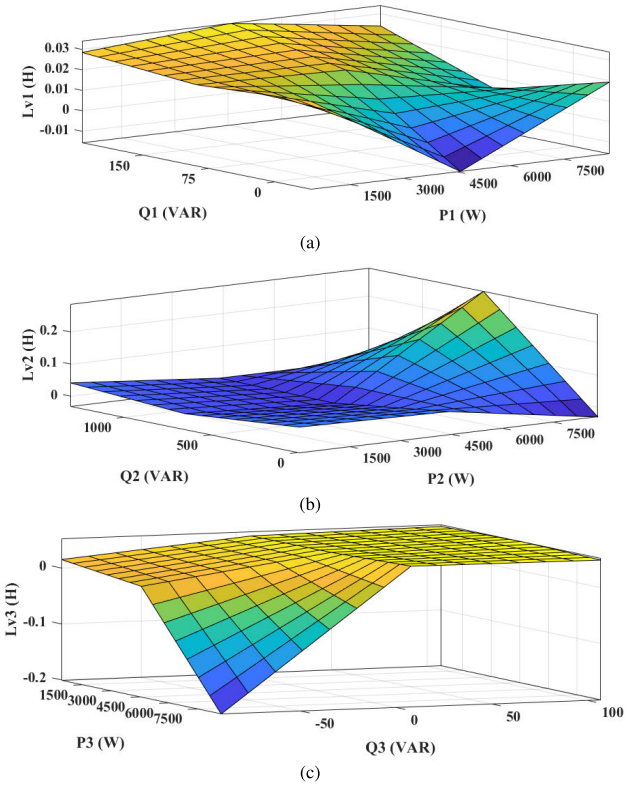

FIGURE 8. The trained ANFIS networks for calculating optimal VIs a) L_{v1}, b) L_{v2}, c) L_{v3}.

The ANFIS network of converter 3 is also depicted in Fig.8c. The maximum values of L_{v3} are corresponding with the minimum active and reactive power injections. There is a breaking point in $P_3 - L_{v3}$ axis so as the rate of change of P_3 before and after $P_3 = 4561.45\ W$ are total different. In active powers lower than this value, the change of virtual inertia is independent from change in active power of converter 3. However, the points over this value present a dramatic change in L_{v3} by changing P_3.

C. LOAD CHANGES SCENARIO

A static load ($R_{pert} + \mathrm{j}.X_{pert}$) is connected to bus 1 at t = 0.5 s, then the same load is switched in bus 2 at t = 1.5 s, and finally a similar load is connected to bus 3 at t = 2.5 s. Different dynamic characteristics are drawn by MATLAB simulation and demonstrated, subsequently. The results obtained by the proposed method are compared with the results achieved by applying the control method in another study [7].

1) FREQUENCY OF THE MICROGRID

The frequency of the microgrid in different buses is shown in Fig.9 using the proposed control method and also the control method in [7]. The frequency fluctuations while applying the proposed control method are negligible in comparison with applying the control method in [7]. The microgrid frequency nadir values are shown in Fig.9 at maximum deviation points. The frequency nadir while applying ANFIS-based control method is 49.9529 Hz while the corresponding value while applying the control method in [7] is 49.9435 Hz. Accordingly, the proposed ANFIS-based control method enhances the frequency nadir.

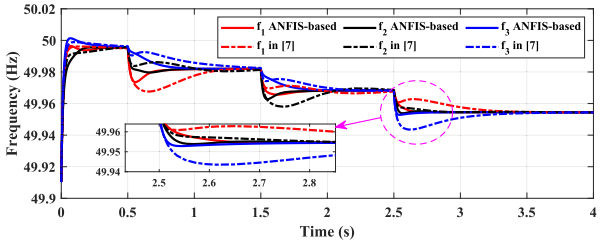

FIGURE 9. The microgrid frequency in load change scenario while applying the proposed ANFIS controller and the control method in [7].

2) VOLTAGE COMPONENTS OF THE MICROGRID

The dq-axis voltage components are demonstrated in Fig.10 while applying the proposed ANFIS-based control method and the control method in [7]. The d-axis voltage components are changing around zero in Fig.10a, either using the ANFIS-based control method or applying the control method in [7] since both methods keep the d-axis voltage at zero. The q-axis voltage components are shown in Fig.10b. As it is seen, the minimum instantaneous voltage while applying the proposed ANFIS-based control method is 370.98 V which is roughly equal to the minimum q-axis voltage while applying [7] (370.22 V). The minimum steady state voltages while applying the proposed control method or the control method in [7] are 380.44 V and 381.02 V, respectively. Consequently, the voltage drops while applying both control methods are roughly identical. Therefore, from the voltage point of view both control methods demonstrate a satisfactory performance.

3) THE MICROGRID OUTPUT CURRENT COMPONENTS

The current components injected by converters 1, 2, and 3 are demonstrated in Fig.11. The d-axis currents in Fig.11a by ANFIS-based control method show lower mismatches and fluctuations than d-axis currents drawn by [7]. The maximum current mismatches in Fig.11a using the proposed ANFIS-based control and using the control method in [7] are 0.37 A and 2.37 A, respectively. Therefore, the ANFIS-based method excelled the control method in [7] in minimizing the d-axis current mismatch. The steady-state values of q-axis current components in Fig.11b are identical, but the current overshoot and fluctuations while applying the ANFIS-based control method are lower than the corresponding values while applying the control method in [7] (3.2381 A and 3.2595 A, respectively). Consequently, the performance of the ANFIS-based control method exceeds the performance of the control method in [7] from the current point of view.

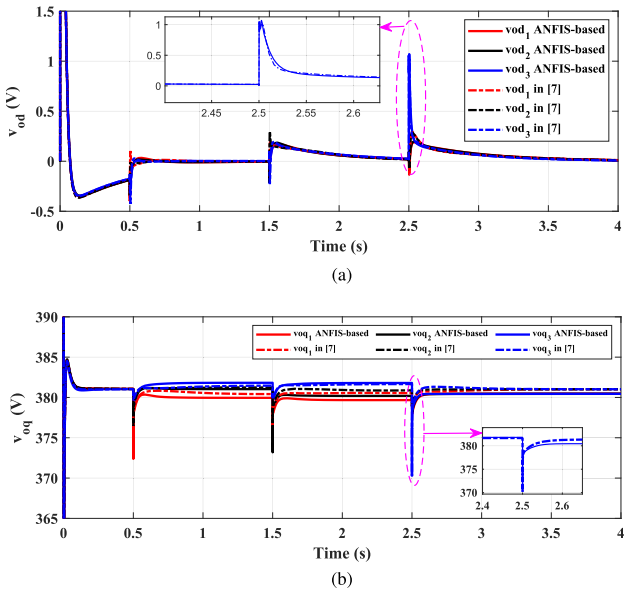

FIGURE 10. The microgrid voltage components for converters 1, 2, 3 in load change scenario while applying the proposed ANFIS controllers and the controller in [7]. a

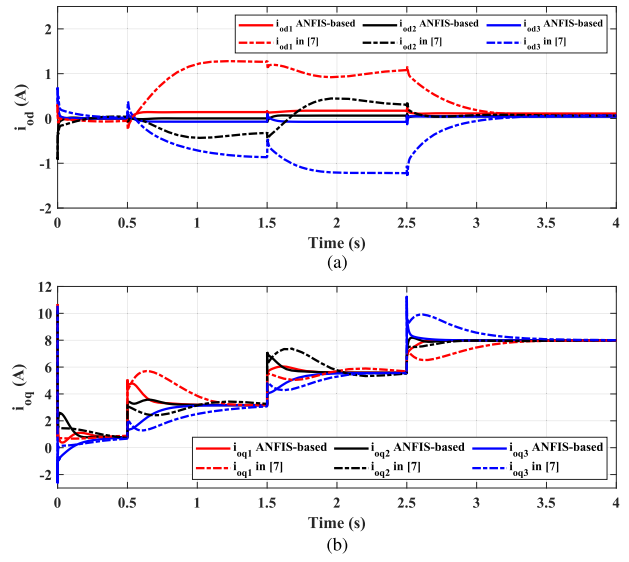

FIGURE 11. The microgrid current components for converters 1, 2, 3 in load change scenario while applying the proposed ANFIS controllers and the controllers in [7].

4) THE CONVERTERS ACTIVE AND REACTIVE POWERS

The active powers injected by converters 1, 2, and 3 are shown in Fig.12a. The steady-state active power values using both methods are 1.74 kW, 3.18 kW, and 4.57 kW at t = 1.5, 2.5, and 3.5 s, respectively. The maximum overshoot in active power curves by the proposed ANFIS-based controller is 0.96 kW and the corresponding value by the control method in [7] is 1.36 kW in Fig.12a. Consequently, the active power overshoot is decreased by the proposed ANFIS-based control method which is a prominent advantage. The reactive powers injected by converters 1, 2, and 3 are shown in Fig.12b. The maximum reactive power mismatches while applying the ANFIS-based controller and the control method in [7] are 0.277 kVAR and 2.74 kVAR, respectively. Therefore the reactive power mismatches are decreased substantially which is a major contribution of the proposed ANFIS-based controller. It should be noted that the ANFIS-based controllers are independent of the load-change location in the microgrid and they can successfully cope with the load changes in three different buses at t = 0.5 s, t = 1.5 s, and t = 2.5 s.

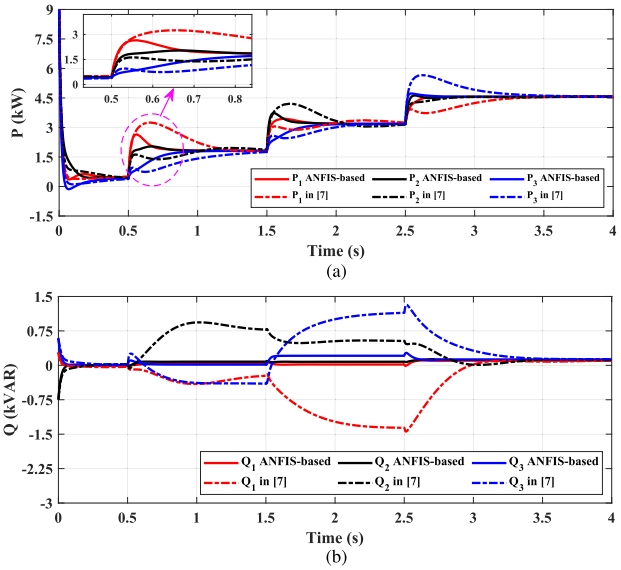

FIGURE 12. The converters active and reactive powers in load change scenario applying the proposed optimal parameters and the corresponding voltage components in [7], a) active power (*P*), b) reactive power (Q).

VI. CONCLUSION

Herein, the dynamic modeling of a converter-interfaced microgrid including static loads, lines and PLL devices has been performed as the first step. An objective function has been defined based on microgrid small-signal stability analysis and reactive power mismatches in the microgrid. The next step has been to define an algorithm to train ANFIS networks which have been new elements applied in the proposed control method. These elements determine the VI values with respect to instantaneous active and reactive powers in the proposed control block diagram. The ANFIS-based method applied PSO algorithm to draw optimal training data in all load scenarios. Finally, the training-data has been completed and this data has been delivered to the ANFIS training step. Trained networks have been installed in the converter controller and a simulation scenario including three successive load changes in the microgrid have been implemented. According to the simulation results, the proposed control method could favorably minimize the reactive power mismatches among converters independent of the load change location. The dynamic responses including the current responses have been enhanced by the proposed control

method. Moreover, the eigenvalues analysis has clarified a prominent advancement in microgrid small-signal stability by applying the proposed control method. The simulation studies validate the applicability and effectiveness of the proposed ANFIS-based control method.

REFERENCES

[1] M. Farrokhabadi, C. A. Cañizares, J. W. Simpson-Porco, E. Nasr, L. Fan, P. A. Mendoza-Araya, R. Tonkoski, U. Tamrakar, N. Hatziargyriou, D. Lagos, and R. W. Wies, "Microgrid stability definitions, analysis, and examples," *IEEE Trans. Power Syst.*, vol. 35, no. 1, pp. 13–29, Jan. 2020.

[2] N. Pogaku, M. Prodanovic, and T. C. Green, "Modeling, analysis and testing of autonomous operation of an inverter-based microgrid," *IEEE Trans. Power Electron.*, vol. 22, no. 2, pp. 613–625, Mar. 2007.

[3] B. Pournazarian, M. Saeedian, B. Eskandari, M. Lehtonen, and E. Pouresmaeil, "Feasible ranges of microgrid parameters based on small-signal stability analysis," in *Proc. IEEE 21st Workshop Control Modeling Power Electron. (COMPEL)*, Nov. 2020, pp. 1–6.

[4] Y. Pan, L. Chen, X. Lu, J. Wang, F. Liu, and S. Mei, "Stability region of droop-controlled distributed generation in autonomous microgrids," *IEEE Trans. Smart Grid*, vol. 10, no. 2, pp. 2288–2300, Mar. 2019.

[5] A. Firdaus and S. Mishra, "Mitigation of power and frequency instability to improve load sharing among distributed inverters in microgrid systems," *IEEE Syst. J.*, vol. 14, no. 1, pp. 1024–1033, Mar. 2020.

[6] Y. Peng, Z. Shuai, X. Liu, Z. Li, J. M. Guerrero, and Z. J. Shen, "Modeling and stability analysis of inverter-based microgrid under harmonic conditions," *IEEE Trans. Smart Grid*, vol. 11, no. 2, pp. 1330–1342, Mar. 2020.

[7] M. Rasheduzzaman, J. A. Mueller, and J. W. Kimball, "An accurate small-signal model of inverter-dominated islanded microgrids using *dq* reference frame," *IEEE J. Emerg. Sel. Topics Power Electron.*, vol. 2, no. 4, pp. 1070–1080, Dec. 2014.

[8] S. Leitner, M. Yazdanian, A. Mehrizi-Sani, and A. Muetze, "Small-signal stability analysis of an inverter-based microgrid with internal model-based controllers," *IEEE Trans. Smart Grid*, vol. 9, no. 5, pp. 5393–5402, Sep. 2018.

[9] Y. Yan, D. Shi, D. Bian, B. Huang, Z. Yi, and Z. Wang, "Small-signal stability analysis and performance evaluation of microgrids under distributed control," *IEEE Trans. Smart Grid*, vol. 10, no. 5, pp. 4848–4858, Sep. 2019.

[10] J. He, X. Wu, X. Wu, Y. Xu, and J. M. Guerrero, "Small-signal stability analysis and optimal parameters design of microgrid clusters," *IEEE Access*, vol. 7, pp. 36896–36909, 2019.

[11] B. K. Unnikrishnan, M. S. Johnson, and E. P. Cheriyan, "Small signal stability improvement of a microgrid by the optimised dynamic droop control method," *IET Renew. Power Gener.*, vol. 14, no. 5, pp. 822–833, Apr. 2020.

[12] S. Wang, Z. Liu, J. Liu, D. Boroyevich, and R. Burgos, "Small-signal modeling and stability prediction of parallel droop-controlled inverters based on terminal characteristics of individual inverters," *IEEE Trans. Power Electron.*, vol. 35, no. 1, pp. 1045–1063, Jan. 2020.

[13] B. Pournazarian, M. Saeedian, M. Lehtonen, S. Taheri, and E. Pouresmaeil, "Microgrid stability analysis considering current state-feedback," in *Proc. IEEE 11th Int. Symp. Power Electron. Distrib. Gener. Syst. (PEDG)*, Sep. 2020, pp. 193–198.

[14] W. Du, Z. Chen, K. P. Schneider, R. H. Lasseter, S. P. Nandanoori, F. K. Tuffner, and S. Kundu, "A comparative study of two widely used grid-forming droop controls on microgrid small-signal stability," *IEEE J. Emerg. Sel. Topics Power Electron.*, vol. 8, no. 2, pp. 963–975, Jun. 2020.

[15] Z. Shuai, Y. Peng, X. Liu, Z. Li, J. M. Guerrero, and Z. J. Shen, "Parameter stability region analysis of islanded microgrid based on bifurcation theory," *IEEE Trans. Smart Grid*, vol. 10, no. 6, pp. 6580–6591, Nov. 2019.

[16] V. N. Kumar and S. K. Parida, "Parameter optimization of universal droop and internal model controller for multi inverter-fed DGs based on accurate small-signal model," *IEEE Access*, vol. 7, pp. 101928–101940, 2019.

[17] J. He and Y. W. Li, "Analysis, design, and implementation of virtual impedance for power electronics interfaced distributed generation," *IEEE Trans. Ind. Appl.*, vol. 47, no. 6, pp. 2525–2538, Nov./Dec. 2011, doi: 10.1109/TIA.2011.2168592.

[18] X. Wu, C. Shen, and R. Iravani, "Feasible range and optimal value of the virtual impedance for droop-based control of microgrids," *IEEE Trans. Smart Grid*, vol. 8, no. 3, pp. 1242–1251, May 2017.

[19] B. Pournazarian, S. S. Seyedalipour, M. Lehtonen, S. Taheri, and E. Pouresmaeil, "Virtual impedances optimization to enhance microgrid small-signal stability and reactive power sharing," *IEEE Access*, vol. 8, pp. 139691–139705, 2020.

[20] A. A. N. Lasheen, M. Ammar, H. H. Zeineldin, A. Al-Durra, M. F. Shaaban, and E. F. El-Saadany, "Assessing the impact of reactive power droop on inverter based microgrid stability," *IEEE Trans. Energy Convers.*, early access, Jan. 19, 2021.

[21] G. N. Baltas, N. B. Lai, L. Marin, A. Tarrasó, and P. Rodriguez, "Grid-forming power converters tuned through artificial intelligence to damp subsynchronous interactions in electrical grids," *IEEE Access*, vol. 8, pp. 93369–93379, 2020.

[22] J.-S. R. Jang, "ANFIS: Adaptive-network-based fuzzy inference system," *IEEE Trans. Syst., Man, Cybern.*, vol. 23, no. 3, pp. 665–685, May/Jun. 1993.

[23] Q. Xu, T. Dragicevic, L. Xie, and F. Blaabjerg, "Artificial intelligence-based control design for reliable virtual synchronous generators," *IEEE Trans. Power Electron.*, vol. 36, no. 8, pp. 9453–9464, Aug. 2021, doi: 10.1109/TPEL.2021.3050197.

[24] H. Bevrani and S. Shokoohi, "An intelligent droop control for simultaneous voltage and frequency regulation in islanded microgrids," *IEEE Trans. Smart Grid*, vol. 4, no. 3, pp. 1505–1513, Sep. 2013.

[25] D. Mlakic, H. R. Baghaee, and S. Nikolovski, "A novel ANFIS-based islanding detection for inverter-interfaced microgrids," *IEEE Trans. Smart Grid*, vol. 10, no. 4, pp. 4411–4424, Jul. 2019.

[26] J. Saroha, M. Singh, and D. K. Jain, "ANFIS-based add-on controller for unbalance voltage compensation in a low-voltage microgrid," *IEEE Trans. Ind. Informat.*, vol. 14, no. 12, pp. 5338–5345, Dec. 2018.

[27] M. R. AlRashidi and M. E. El-Hawary, "A survey of particle swarm optimization applications in electric power systems," *IEEE Trans. Evol. Comput.*, vol. 13, no. 4, pp. 913–918, Aug. 2009.

BAHRAM POURNAZARIAN (Student Member, IEEE) received the B.Sc. degree in electrical power engineering from Razi University, Kermanshah, Iran, in 2012, and the M.Sc. degree in electrical power engineering from the Amirkabir University of Technology (Tehran Polytechnic), Tehran, Iran, in 2016. He is currently pursuing the Ph.D. degree in power electronics engineering with Aalto University, Espoo, Finland. His research interests include micogrids modeling, control and stability, grid integration of renewable energy sources, and heuristic optimization algorithms.

REZA SANGRODY received the B.Sc. and M.Sc. degrees in electrical engineering from the University of Mazandaran, in 2003 and 2005, respectively.

Since 2005, he has been with Islamic Azad University, Firoozkooh Branch, as a Lecturer. Since 2012, he has also been a Consultant Engineer working with Behjosh Electric Factory for designing and producing different types of welding machines. He has published more than 20 journal articles and conference papers in the field of power electronics applications. His current research interests include power electronic circuit design and control; application of power electronic converter in smart grid, photovoltaic, and wind energy harvesting; and electrical machines drivers design and control.

MEYSAM SAEEDIAN was born in 1991. He received the B.Sc. degree in electrical engineering from the Arak University of Technology, Arak, Iran, in 2014, and the M.Sc. degree from the Babol Noshirvani University of Technology, Babol, Iran, in 2017. He is currently pursuing the Ph.D. degree with the Department of Electrical Engineering and Automation, Aalto University, Espoo, Finland. His research interests include the design of power electronic converters, control systems, grid voltage and frequency stability, and RES integration.

ORIOL GOMIS-BELLMUNT (Fellow, IEEE) received the degree in industrial engineering from the School of Industrial Engineering of Barcelona (ETSEIB), Technical University of Catalonia (UPC), Barcelona, Spain, in 2001, and the Ph.D. degree in electrical engineering from UPC, in 2007. In 1999, he joined Engitrol S.L., where he worked as a Project Engineer in the automation and control industry. Since 2004, he has been with the Department of Electrical Engineering, UPC, where he is currently a Professor and participates in the CITCEA-UPC Research Group. Since 2020, he is an ICREA Academia Researcher. His research interests include the fields linked with electrical machines, power electronics, and renewable energy integration in power systems.

EDRIS POURESMAEIL (Senior Member, IEEE) received the Ph.D. degree in electrical engineering from the Technical University of Catalonia (UPC) (BarcelonaTech), Barcelona, Spain, in 2012. After his Ph.D., he joined the University of Waterloo, Waterloo, Canada, as a Postdoctoral Research Fellow, and then joined the University of Southern Denmark (SDU), Odense, Denmark, as an Associate Professor. He is currently an Associate Professor with the Department of Electrical Engineering and Automation (EEA), Aalto University, Espoo, Finland. His main research activities focus on the application of power electronics in power and energy sectors.